mathematics

MDPI

Article

Micromechanics-Based Strength Criterion for Root-Reinforced Soil

Wei Luo [1,2], Fu Cao [3,*], Yang Wang [1], Guiyou Xiao [1] and Enlong Liu [2,*]

[1] Tibet Development Investment Group Co., Ltd., Lhasa 851414, China; 18980665300@163.com (W.L.); 18223956483@163.com (Y.W.); xguiyou1993@163.com (G.X.)
[2] State Key Laboratory of Hydraulics and Mountain River Engineering, College of Water Resource & Hydropower, Sichuan University, Chengdu 610065, China
[3] PowerChina HydroPower Development Group Co., Ltd., Chengdu 610041, China
* Correspondence: sclfcaofu@powerchina.cn (F.C.); liuenlong@scu.edu.cn (E.L.)

Abstract

To address the limitation of using experimental parameters in the macroscopic strength criterion, a micromechanical strength criterion for root-reinforced soil is developed. In this model, a micromechanical model for a three-phase composite ("root—cemented soil matrix—frictional element") is constructed, and the novel combination of energy equivalence principles with the M-T method is used to determine the meso-scale prestress and strength criterion for root-reinforced soil under freeze–thaw cycles. The representative volume element (RVE) of root-reinforced soil is conceptualized as a composite material consisting of a bonded element (a cemented-soil matrix with root inclusions) and frictional inclusions. By applying micromechanics, along with the Mori–Tanaka method, the LCC method, limit analysis theory, and macro–micro energy equivalence principles (incorporating both strain and dissipated energy), a micromechanical strength criterion is formulated, revealing failure mechanisms at the microscale. The previously used stepwise procedure for deriving the stationary function is improved, and the microscale prestress is determined through the Mori–Tanaka method combined with macro–micro strain-energy equivalence. The proposed micromechanical strength criterion effectively models the primary strength variation in root-reinforced soil under freeze–thaw cycles, extending the existing shear criterion for soil.

Keywords: root-reinforced; soil; freeze-thaw cycles; strength criterion; micromechanics

MSC: 74E20; 74E99

check for updates

Academic Editor: Yumin Cheng

Received: 12 October 2025
Revised: 26 November 2025
Accepted: 1 December 2025
Published: 4 December 2025

Citation: Luo, W.; Cao, F.; Wang, Y.; Xiao, G.; Liu, E. Micromechanics-Based Strength Criterion for Root-Reinforced Soil. *Mathematics* **2025**, *13*, 3890. https://doi.org/10.3390/math13233890

Copyright: © 2025 by the authors. Licensee MDPI, Basel, Switzerland. This article is an open access article distributed under the terms and conditions of the Creative Commons Attribution (CC BY) license (https://creativecommons.org/licenses/by/4.0/).

1. Introduction

Strength theory is used to determine whether a material will fail under various complex stress states, which are widely employed in engineering analysis (slope stability). Current strength criteria are mainly divided into two categories: macroscopic and microscopic. Each has its own characteristics. Research on macroscopic strength criteria started early and is diverse: some involve few parameters with clear physical meaning but have limited general applicability; others involve more parameters yet are broadly applicable; and still others lack clear physical meaning but work well for a particular type of soil. Most macroscopic strength criteria are derived from empirical experimental relations and can generally describe the strength characteristics of a given type of soil well, but they struggle to capture the underlying failure and strength mechanisms. Microscopic strength criteria

consider the microscale features of the constituents, have clearer physical meaning, can better describe soils' failure and strength mechanisms, and help elucidate the essence of soil strength; however, their formulations are cumbersome, making them inconvenient for practical engineering use, and their mesoscopic parameters are generally difficult to obtain with existing testing techniques. Research on microscopic strength criteria is still in its infancy and requires further study to improve their reliability, applicability, and theoretical rigor.

The strength of root-reinforced soils is often influenced by multiple factors, including soil types, root species, root architecture (e.g., root-clump shape), root content, and soil water content. In the tests of Wan et al. [1], Lian et al. [2], and Feng et al. [3], roots were found to significantly increase cohesion while having almost no effect on the internal friction angle. Wang et al. [4] reached similar conclusions for undisturbed grass-rooted soils and, in tests on remolded grass-rooted soils, found an optimal root content that maximizes reinforcement. For the remolded grass-rooted soils, the parameters obtained cannot be used in the design, in practice. Hamidifar et al. [5] reported that roots of vetiver grass can markedly improve soil strength indices, increasing cohesion by 119.6% and the internal friction angle by 81.96%. Maffra et al. [6] tested rooted and root-free soil samples from Atlantic Forest plantations and found that the strengthening effect also depends on soil type: in sandy soils, roots influence strength mainly through cohesion (increasing it by up to 234%), whereas in clays, both cohesion (32%) and internal friction angle (14.4%) increased; in addition, other researchers also studied the effect of roots on sandy soils and obtained similar conclusions [7,8]. Field shear tests by Fan and Su [9] showed that as soil water content rises, the shear strength of rooted soils decreases significantly. Liu et al. [10] studied the soil-stabilizing effect of mixed-species root systems on saline loess slopes, finding that both cohesion and internal friction angle decreased linearly with increasing water content. Rooted soil cohesion increased linearly with biomass density, peaking when the root mass ratio (RMR) was 0.6 and salt content was 1.18%, before decreasing. The internal friction angle initially increased with biomass density, then decreased, with a turning point at 0.015 g/cm^3. The relationship between internal friction angle and RMR was exponential, while it was linear and subtractive with salt content. Gonzalez-Ollauri and Mickovski [11], examining root reinforcement under different hydrological conditions, found a pronounced increase in internal friction angle and proposed the existence of an optimal soil water content. Overall, even though vegetation may exert some negative effects on soils, balancing the various positive and negative influences leads to the conclusion that plant roots can effectively enhance soil strength, except under extreme conditions, such as surface layers with particularly high organic content.

Regarding the effects of freeze–thaw cycling on soil strength, in addition to those mentioned earlier, many scholars have conducted related studies on different soils. Using a basaltic soft clay recycled with gypsum byproduct as the test material, Kamei et al. [12], and focusing on gypseous soils, Aldaood et al. [13], both found that freeze–thaw cycles reduce unconfined compressive strength and durability. Han et al. [14] investigated how freeze–thaw cycles affect the mechanical properties and strength indices of saline soils in western Jilin, grouping test conditions into relatively undamaged, single-factor damage, and dual-factor damage, and proposed an empirical equation with high reliability ($R^2 > 0.985$) to describe the combined effects of freeze–thaw cycles and salinity on strength indices. Ma et al. [15] examined the dynamic properties of mudstone and sandy mudstone after freeze–thaw cycling, defining two parameters—the dynamic coefficient of freeze–thaw damage and the freeze–thaw damage variable—and found that, for the same number of cycles, mudstone exhibits a higher dynamic coefficient of freeze–thaw damage. Xu et al. [16] studied the combined effects of freeze–thaw erosion and salt erosion on the strength of loess

in northwest China; during the first five freeze–thaw cycles, the ratio of the freeze–thaw damage coefficient to the salt-erosion damage coefficient decreased as cycling progressed, and after more than five cycles, both the freeze–thaw damage coefficient and cohesion decayed to a stable level. Qu et al. [17], working with cohesive coarse-grained soils from slopes along the Qinghai–Tibet region, found that the number of freeze–thaw cycles is negatively correlated with uniaxial compressive strength, residual strength, elastic modulus, and softening modulus.

To address the nonlinear degradation of frozen soil strength, Fish [18] proposed a parabolic strength criterion, and Chen et al. [19] proposed an elliptical criterion. Liao et al. [20] presented a strength criterion based on a modified critical state framework. Liu et al. [21] categorized existing strength criteria into three classes and developed a new double-shear strength criterion. Luo et al. [22] proposed a strength criterion for glacial till based on a binary medium model. Research on meso-scale strength criteria started relatively late. Zhou and Meschke [23] proposed a micromechanical homogenization approach using the Mori–Tanaka method [24] and the Linear Comparison Composite approach (LCC) [25], treating soil particles as the matrix and ice and water as inclusions, accounting for meso-scale prestress, and derived a meso-scale strength criterion for saturated frozen soils.

The shear strength indices of root-reinforced soils are the key design parameters that characterize failure in slope engineering. Currently, there are two main approaches to shear strength criteria for rooted soils. One approach explicitly separates the reinforcing effect of roots and superposes it on the soil's inherent strength; this reinforcement is influenced by multiple factors such as plant species, root content, root diameter, root surface area index, spatial distribution pattern, and depth. The Wu–Waldron model and numerous improvements based on it are representative of this approach. The other approach treats the roots and soil as an integrated whole—the root–soil composite—and analyzes the overall medium using geotechnical strength theory, with the root reinforcement implicitly embedded in the corresponding parameters. From a micromechanical perspective, this paper considers interactions between roots and soil particles and, using the macro–micro energy equivalence principle together with the Mori–Tanaka method, develops a strength criterion for rooted soils under freeze–thaw cycling. Compared with existing micromechanical models [23], we do not consider the plant root system as a key reinforcing phase; this work provides a theoretical design basis for geotechnical engineering involving root-reinforced soils experiencing freezing–thawing actions.

2. Conceptual Framework for Constructing the Strength Criterion

Test results show that the shear strength of root-reinforced soils is influenced not only by confining pressure but also by root content and the number of freezing–thaw cycles [26]. If the rooted soil is treated as a single stress element, the interaction between roots and soil cannot be captured. As shown in Figure 1, at the macroscopic scale, the bonded element is taken as the matrix and the frictional element as the inclusion; a binary-medium representative volume element (RVE) is thus formed by bonded and frictional elements. At the mesoscopic scale, the bonded element itself consists of a cemented-soil matrix with root inclusions.

Through two homogenization steps, this model yields a strength criterion for rooted soils from the micro- to the macro-scale; a schematic of the homogenization procedure is given in Figure 2.

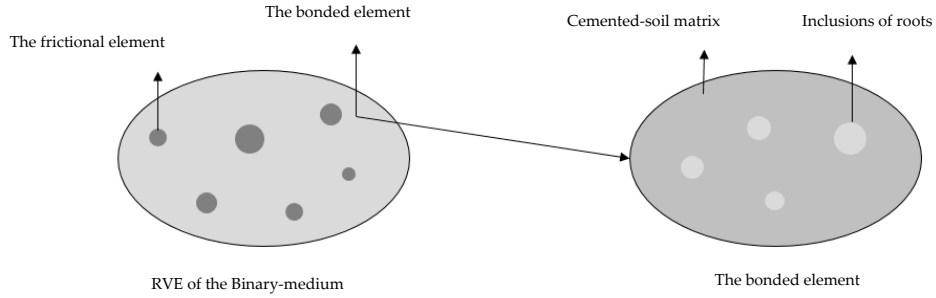


Figure 1. Schematic of the meso-scale binary-medium model of root-reinforced soil.

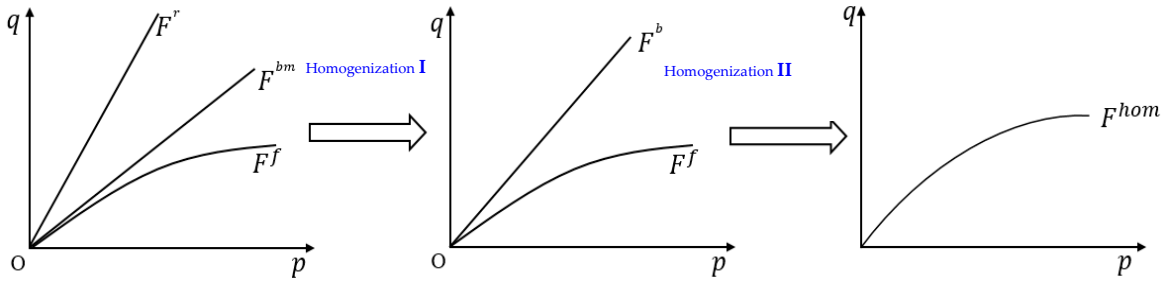


Figure 2. Schematic of the homogenization steps for the strength criterion of root-reinforced soil.

(i) Homogenization I: Homogenizing the cemented-soil matrix with the root inclusions gives the strength criterion F^b for the bonded element. Both the cemented-soil matrix and the roots are modeled as linear elastic, and their strength criteria have the same form. Therefore, an elastic homogenization approach can be used directly to establish the strength criterion of the bonded element, which retains a linear character after homogenization.

(ii) Homogenization II: Homogenizing the bonded and frictional elements yields the macroscopic strength criterion for the rooted soil. The frictional element follows a nonlinear elasto-plastic constitutive model; plastic dissipation occurs during loading, and its strength criterion F^f is nonlinear. In addition, during the homogenization of bonded and frictional elements, energy transfer caused by the breakage of the bonded elements must be considered; this includes both strain energy and dissipated energy. When some bonded elements fail and transform into frictional elements, additional energy dissipation occurs—analogous to the breakage of particle agglomerates—which is an energy-transfer process that must be accounted for in homogenization.

3. Strength Criterion

3.1. Strength Criterion for the Bonded Element (Homogenization I)

The stress refers to the effective stress, and the stress in compression is positive. We define the mean stress p, generalized shear stress q, volumetric strain ε_v, and generalized shear strain ε_s as follows:

$$\boldsymbol{\sigma} = p\mathbb{I} + \boldsymbol{s} \tag{1}$$

$$p = tr\boldsymbol{\sigma}/3 \tag{2}$$

$$q = \sqrt{3(\boldsymbol{s} : \boldsymbol{s})/2} \tag{3}$$

$$\boldsymbol{\varepsilon} = \varepsilon_v\mathbb{I} + \boldsymbol{e} \tag{4}$$

$$\varepsilon_v = tr\boldsymbol{\varepsilon}/3 \tag{5}$$

$$\varepsilon_s = \sqrt{2(\boldsymbol{e} : \boldsymbol{e})/3} \tag{6}$$

where $\mathbb{I}$ is the unit tensor; $\boldsymbol{\sigma}$ and $\boldsymbol{\varepsilon}$ are, respectively, stress and strain tensor; and $\boldsymbol{s}$ and $\boldsymbol{e}$ are, respectively, deviatoric stress and deviatoric strain tensor. Under triaxial stress conditions with $\sigma_1 > \sigma_2 = \sigma_3$, $p = (\sigma_1 + 2\sigma_3)/3$, and $q = \sigma_1 - \sigma_3$, σ_1 and σ_3 denote the maximum and minimum principal stress, respectively. When expressing the strength criterion using Mohr–Coulomb, $\tau = c + \sigma \tan \varphi$, c and φ are the strength parameters of cohesion and internal frictional angle, respectively, and they can also be expressed in terms of p and q as follows: $q = \frac{6c \cdot co\varphi}{3 - sin\varphi} + \frac{6sin\varphi}{3 - sin\varphi} p$.

We define the strength for cemented-soil matrix F^{bm} and roots inclusion F^r, respectively, as follows:

$$F^{bm} = q^{bm} - k^{bm} p^{bm} = 0 \tag{7}$$

$$F^r = q^r - k^r p^r = 0 \tag{8}$$

where q^{bm} and p^{bm} denote the principal stress difference and mean stress, respectively, of the cemented-soil matrix at the failure state; q^r and p^r denote the principal stress difference and mean stress, respectively, of the root inclusions at the failure state; k^{bm} and k^r are the corresponding strength parameters. The strength parameters can be expressed as follows:

$$k^{bm} = \frac{q^{bm}}{p^{bm}} = \frac{3G^{bm}}{K^{bm}} \tag{9}$$

$$k^r = \frac{q^r}{p^r} = \frac{3G^r}{K^r} \tag{10}$$

where K^{bm} and G^{bm} are the bulk and shear moduli, respectively, of the cemented-soil matrix at the failure state; and K^r and G^r are the bulk and shear moduli, respectively, of the root inclusions at the failure state.

In a root–soil mixture, take a representative volume element (RVE). The volumes of its parts satisfy the following:

$$V = V^b + V^f \tag{11}$$

$$V^b = V^{bm} + V^r \tag{12}$$

where V, V^b, V^f, V^{bm}, and V^r denote the volumes of the RVE, the bonded element, the frictional element, the cemented-soil matrix, and the root inclusion, respectively.

Define $\lambda^f = V^f/V$ as the breakage ratio (volume fraction of the frictional element) and $\lambda^r = V^r/V$ as the root volume fraction of the specimen (hereafter referred to as the root content). The volume fraction of roots within the bonded element, λ^{br}, is as follows:

$$\lambda^{br} = \frac{V^r}{V^{bm} + V^r} = \frac{\lambda^r}{1 - \lambda^f} \tag{13}$$

Within the bonded element, by the theory of volumetric homogenization, the stresses and strains of the cemented-soil matrix and the root inclusion satisfy the following:

$$\boldsymbol{\sigma}^b = \left(1 - \lambda^{br}\right) \boldsymbol{\sigma}^{bm} + \lambda^{br} \boldsymbol{\sigma}^r \tag{14}$$

$$\boldsymbol{\varepsilon}^b = \left(1 - \lambda^{br}\right) \boldsymbol{\varepsilon}^{bm} + \lambda^{br} \boldsymbol{\varepsilon}^r \tag{15}$$

where $\boldsymbol{\sigma}^b$ and $\boldsymbol{\varepsilon}^b$ are the stress and strain tensors of the bonded element; $\boldsymbol{\sigma}^{bm}$ and $\boldsymbol{\varepsilon}^{bm}$ are those of the cemented-soil matrix; and $\boldsymbol{\sigma}^r$ and $\boldsymbol{\varepsilon}^r$ are those of the root inclusion.

Treating the cemented soil as the matrix and the roots as inclusions within the bonded element, both micromechanics and the Mori–Tanaka method give the following:

$$\boldsymbol{\varepsilon}^r = \mathbb{A}^r : \boldsymbol{\varepsilon}^b \tag{16}$$

$$\mathbb{A}^r = \left[\mathbb{I} + \mathbb{S}^{bm} : \left(\mathbb{C}^{bm}\right)^{-1} : \left(\mathbb{C}^r - \mathbb{C}^{bm}\right)\right]^{-1} \tag{17}$$

where $\mathbb{C}^{bm}$ and $\mathbb{C}^{bm}$ are the stiffness tensors of the cemented-soil matrix and the root inclusion, respectively [27–30]. The derivation process of (17) can be found in Appendix A. The Eshelby tensor of the bonded element with cemented soil as matrix is as follows:

$$\mathbb{S}^{bm} = S_1^{bm}\mathbb{J} + S_2^{bm}\mathbb{K} \tag{18a}$$

$$S_1^{bm} = \frac{3K^{bm}}{3K^{bm} + 4G^{bm}} \tag{18b}$$

$$S_2^{bm} = \frac{6}{5}\frac{K^{bm} + 2G^{bm}}{3K^{bm} + 4G^{bm}} \tag{18c}$$

where K^{bm} and G^{bm} are the volumetric and shear moduli of the cemented-soil matrix.

Both the cemented-soil matrix and the root inclusion obey linear elastic constitutive laws (Hooke's law). The constitutive relation and stiffness tensor $\mathbb{C}^{bm}$ of the cemented-soil matrix are, respectively, as follows:

$$d\boldsymbol{\sigma}^{bm} = \mathbb{C}^{bm} : d\boldsymbol{\varepsilon}^{bm} \tag{19}$$

$$\mathbb{C}^{bm} = 3K^{bm}\mathbb{J} + 2G^{bm}\mathbb{K} \tag{20}$$

The constitutive relation and stiffness tensor $\mathbb{C}^r$ of the roots are, respectively, as follows:

$$d\boldsymbol{\sigma}^r = \mathbb{C}^r : d\boldsymbol{\varepsilon}^r \tag{21}$$

$$\mathbb{C}^r = 3K^r\mathbb{J} + 2G^r\mathbb{K} \tag{22}$$

Solving Equations (13)–(22) jointly yields the following:

$$\boldsymbol{\sigma}^{bm} = \mathbb{D}^{bm} : \boldsymbol{\sigma}^b \tag{23}$$

$$\mathbb{D}^{bm} = \left[\left(1 - \lambda^{br}\right)\mathbb{I} + \lambda^{br}\mathbb{C}^r : \mathbb{A}^r : \left(\mathbb{C}^{\boldsymbol{b}}\right)^{-1}\right]^{-1} \tag{24a}$$

and $\mathbb{C}^b$ is the effective stiffness tensor of the composite material of the cemented-soil matrix and the root inclusion, having $d\boldsymbol{\sigma}^b = \mathbb{C}^b : d\boldsymbol{\varepsilon}^b$, and the following:

$$\mathbb{C}^b = \left[\left(1 - \lambda^{br}\right)\mathbb{C}^{bm} + \lambda^{br}\mathbb{C}^r\mathbb{A}^{\boldsymbol{r}}\right] : \left[\left(1 - \lambda^{br}\right)\mathbb{I} + \lambda^{br}\mathbb{A}^{\boldsymbol{r}}\right]^{-1} \tag{24b}$$

$$\boldsymbol{\sigma}^r = \mathbb{D}^r : \boldsymbol{\sigma}^b \tag{25}$$

$$\mathbb{D}^r = \left[\mathbb{I} - \left(1 - \lambda^{br}\right)\mathbb{D}^{bm}\right]/\lambda^{br} \tag{26}$$

where $\mathbb{D}^{bm}$ and $\mathbb{D}^r$ are the local stress concentration tensors of the cemented-soil matrix and the roots, respectively, and the derivation process in detail can be found in Appendix A.

From tensor algebra, any isotropic fourth-order tensor can be expressed as a linear combination of the spherical and deviatoric fourth-order identity tensors. By reducing the fourth-order tensor expressions to second-order matrix form, and since both the cemented-soil matrix and the root inclusions follow linear elastic constitutive models, the resulting second-order matrices are diagonal. After computing the above tensors and simplifying, they can be written as follows:

$$\mathbb{S}^{\boldsymbol{bm}} = \left(S_{\mathbf{1}}^{bm}, S_{\mathbf{2}}^{bm}\right) \tag{27}$$

$$\mathbb{C}^{bm} = \left(K^{bm}, 3G^{bm}\right) \tag{28}$$

$$\mathbb{C}^{r} = \left(K^{r}, 3G^{r}\right) \tag{29}$$

$$\mathbb{A}^{r} = \left(\mathbb{A}_1^{r}, \mathbb{A}_2^{r}\right) = \left(\frac{K^{bm}}{K^{bm} + S_1^{bm}\left(K^{r} - K^{bm}\right)}, \frac{G^{bm}}{G^{bm} + S_2^{bm}\left(G^{r} - G^{bm}\right)}\right) \tag{30}$$

$$\mathbb{D}^{bm} = \left(\mathbb{D}_1^{bm}, \mathbb{D}_2^{bm}\right) \tag{31a}$$

$$\mathbb{D}_1^{bm} = \frac{K^{bm} + S_1^{bm}\left(K^{r} - K^{bm}\right)}{K^{bm} + \left(S_1^{bm} + \lambda^{br} - S_1^{bm}\lambda^{br}\right)\left(K^{r} - K^{bm}\right)} \tag{31b}$$

$$\mathbb{D}_2^{bm} = \frac{G^{bm} + S_2^{bm}\left(G^{r} - G^{bm}\right)}{G^{bm} + \left(S_2^{bm} + \lambda^{br} - S_2^{bm}\lambda^{br}\right)\left(G^{r} - G^{bm}\right)} \tag{31c}$$

$$\mathbb{D}^{r} = \left(\mathbb{D}_1^{r}, \mathbb{D}_2^{r}\right) = \left(\frac{1 - \left(1 - \lambda^{br}\right)\mathbb{D}_1^{bm}}{\lambda^{br}}, \frac{1 - \left(1 - \lambda^{br}\right)\mathbb{D}_2^{bm}}{\lambda^{br}}\right) \tag{32}$$

At the critical state, Equation (14) can be rewritten as the following expression through the mean stress and generalized shear stress:

$$p^{b} = \left(1 - \lambda^{br}\right)p^{bm} + \lambda^{br}p^{r} \tag{33}$$

$$q^{b} = \left(1 - \lambda^{br}\right)q^{bm} + \lambda^{br}q^{r} \tag{34}$$

Substituting Equations (7) and (8) into Equation (34), we can obtain the following:

$$q^{b} = \left(1 - \lambda^{br}\right)k^{bm}p^{bm} + \lambda^{br}k^{r}p^{r} \tag{35}$$

From Equations (23) and (25), we have the following:

$$p^{bm} = \mathbb{D}_1^{bm}p^{b} \tag{36}$$

$$p^{r} = \mathbb{D}_1^{r}p^{b} \tag{37}$$

Substituting the above two equations into Equation (35), we have the following:

$$q^{b} - \left[\left(1 - \lambda^{br}\right)k^{bm}\mathbb{D}_1^{bm} + \lambda^{br}k^{r}\mathbb{D}_1^{r}\right]p^{b} = 0 \tag{38}$$

The above equation is the strength criterion of the bonded element, which can be rewritten as the following expression:

$$F^{b} = q^{b} - k^{b}p^{b} = 0 \tag{39}$$

$$k^{b} = \left(1 - \lambda^{br}\right)k^{bm}\mathbb{D}_1^{bm} + \lambda^{br}k^{r}\mathbb{D}_1^{r} \tag{40}$$

It can be seen that the bonded element shares the same mathematical form as the cemented-soil matrix and the root inclusions. Since both the cemented-soil matrix and the root inclusions follow linear elastic constitutive models, the bonded element is a linear combination of the cemented-soil matrix and the root inclusions, which is consistent with linear superposition in elasticity.

The bonded element is a linear elastic material. Prior to damage, it undergoes only elastic deformation without plastic deformation. During loading, only the strain energy of

the bonded element changes, with no plastic dissipation. Therefore, at the point of failure, the strain energy φ^b and dissipation energy π^b of the bonded element are as follows:

$$\varphi^b = \frac{1}{2}\boldsymbol{\varepsilon}^b : \mathbb{C}^b : \boldsymbol{\varepsilon}^b = \frac{1}{2}K^b\left(\varepsilon_v^b\right)^2 + \frac{3}{2}G^b\left(\varepsilon_s^b\right)^2 \tag{41}$$

$$\pi^b = 0 \tag{42}$$

Here, ε_v^b and ε_s^b are the volumetric and shear strains of the bonded element at failure; K^b and G^b are the bulk and shear moduli of the bonded element, which can be obtained via the Mori–Tanaka method or another mesomechanics-based approach:

$$K^b = K^{bm}\left[1 + \frac{\lambda^{br}\left(\frac{K^r}{K^{bm}} - 1\right)}{1 + \left(1 - \lambda^{br}\right)S_1^{bm}\left(\frac{K^r}{K^{bm}} - 1\right)}\right] \tag{43}$$

$$G^b = G^{bm}\left[1 + \frac{\lambda^{br}\left(\frac{G^r}{G^{bm}} - 1\right)}{1 + \left(1 - \lambda^{br}\right)S_2^{bm}\left(\frac{G^r}{G^{bm}} - 1\right)}\right] \tag{44}$$

The linear elastic constitutive model of the bonded element is as follows:

$$\mathbb{C}^b = \left(K^b, 3G^b\right) \tag{45}$$

The nonlinear function Υ^b of the bonded element can be written as follows:

$$\Upsilon^b = stat\left(\pi^b - \varphi^b\right) \tag{46}$$

Here, stat(·) denotes the stationarity operator, i.e., taking the extremum of the function in parentheses. By setting the partial derivatives of the variables to zero at the stationary point and solving the resulting coupled equations, the solution can be obtained.

3.2. Strength Criterion for the Frictional Element

From a micromechanical perspective, failure of granular soils is primarily caused by frictional sliding and shear slip [31], exhibiting pronounced elastoplastic deformation characteristics. The strength of the frictional element is nonlinear, and the failure of soil particles can be well described by either the Mohr–Coulomb strength criterion or an elastoplastic strength criterion. For greater generality, this paper adopts an elliptical strength criterion to represent the strength of the frictional element, namely, the following:

$$F^f = 1 - \frac{\left(p^f + S\right)^2}{a} + \frac{\left(q^f\right)^2}{aM^2} = 0 \tag{47}$$

where q^f and p^f are the principal stress difference and mean stress of the frictional element at the critical state; S and M are strength parameters; a is a regularization parameter. As a $\to 0$, $F^f = q^f - M\left(p^f + S\right)$, and the elliptical strength criterion degenerates to the D–P criterion.

Because the frictional element undergoes nonlinear elastoplastic deformation during loading, in addition to the conversion of strain energy, plastic dissipation also occurs. The strain energy of the frictional element is nonlinear and difficult to solve directly. Here, we employ the Linear Comparison Composite (LCC) method [23,32–34] to linearize the constitutive model and obtain an approximate solution for the strain energy. The LCC method refers to linearizing nonlinear features when the components of a composite share similar underlying structures; the nonlinear function Y is a "stationary estimate" of the

difference between the microscale maximum dissipation energy π and the strain energy φ^b of each constituent.

The constitutive model of the frictional element, after LCC-based approximation, is expressed as follows:

$$\boldsymbol{\sigma}^f = \boldsymbol{\tau}^f + C^f : \boldsymbol{\varepsilon}^f = \mathbb{C}^f : \boldsymbol{\varepsilon}^f \tag{48}$$

where $\boldsymbol{\sigma}^f$ and $\boldsymbol{\varepsilon}^f$ are the stress and strain tensors of the frictional element; $\boldsymbol{\tau}^f$ is the prestress tensor of the frictional element; C^f is the elastic stiffness tensor of the friction element, and $\mathbb{C}^f$ is the elastic stiffness of the friction element after linearization; they satisfy, respectively, the following:

$$C^f = \left(K^f, 3G^f\right) \tag{49}$$

$$\mathbb{C}^f = \left(\mathbb{K}^f, 3\mathbb{G}^f\right) \tag{50}$$

The prestress $\boldsymbol{\tau}^f$ is due to the microplastic strain in the frictional elements [35–37], and at the critical failure point, the prestress satisfies the following:

$$\boldsymbol{\tau}^f = C^\tau : \boldsymbol{\varepsilon}^f \tag{51}$$

where C^τ is the prestress stiffness tensor or the linearly corrected stiffness tensor of the friction element, and hence, the following:

$$C^\tau = \mathbb{C}^f - C^f = (K^{\boldsymbol{\tau}}, 3G^{\boldsymbol{\tau}}) \tag{52}$$

Regarding the prestress, some researchers directly assume a specific form, while others determine it via limit analysis by setting partial derivatives to zero. In this paper, it is obtained using the macro–meso energy equivalence principle and the Mori–Tanaka method.

Then, the strain energy φ^f of the friction element can be expressed as follows:

$$\varphi^f = \frac{1}{2}\boldsymbol{\varepsilon}^f : C^f : \boldsymbol{\varepsilon}^f + \boldsymbol{\tau}^f : \boldsymbol{\varepsilon}^f = \frac{1}{2}K^f\left(\varepsilon_v^f\right)^2 + \frac{3}{2}G^f\left(\varepsilon_s^f\right)^2 + \tau_v^f\varepsilon_v^f + \tau_s^f\varepsilon_s^f \tag{53}$$

where K^f and G^f denote the elastic bulk modulus and elastic shear modulus of the friction element; ε_v^f and ε_v^f are the volumetric strain and shear strain of the friction element at failure; τ_v^f and τ_s^f are the volumetric prestress and shear prestress of the friction element.

For the dissipated energy of the friction element, we first define a support function to represent, from a mesoscopic perspective, the maximum energy dissipation associated with the resistance of geomaterials to deformation [35,36,38], namely the following:

$$\pi^f = sup\left(\boldsymbol{\sigma}^f : \boldsymbol{\varepsilon}^{fp}\right) = p^f\varepsilon_v^{fp} + q^f\varepsilon_s^{fp} \tag{54}$$

where ε_v^{fp} and ε_s^{fp} are the plastic volumetric strain and plastic shear strain of the friction element at failure. The plastic strain of the friction element can be written as follows:

$$\boldsymbol{\varepsilon}^{fp} = \boldsymbol{\varepsilon}^f - \boldsymbol{\varepsilon}^{fe} = \left(\mathbb{C}^f\right)^{-1} : \boldsymbol{\sigma}^f - \left(C^f\right)^{-1} : \boldsymbol{\sigma}^f = \left[\left(\mathbb{C}^f\right)^{-1} - \left(C^f\right)^{-1}\right] : \boldsymbol{\sigma}^f \tag{55}$$

The nonlinear function Y^f of the friction element is given by the following:

$$Y^f = stat\left(\pi^f - \varphi^f\right) \tag{56}$$

3.3. Dissipated Energy During the Breakage Process

During the gradual failure of a bonded element and its transition into a friction element, energy is both converted and dissipated; this process can be characterized by a breakage stress [34]. It can be considered that, in the transition from a bonded element to a friction element, energy dissipation predominates. Define the breakage stress $\boldsymbol{\sigma}^{bf}$ as follows:

$$\boldsymbol{\sigma}^{bf} = \boldsymbol{\sigma}^{f} - \boldsymbol{\sigma}^{b} \tag{57}$$

The bonded element deforms linearly and elastically, and only the friction element undergoes plastic deformation during loading. Therefore, the plastic strain of the breakage process $\boldsymbol{\varepsilon}^{bfp}$ is taken to be the plastic strain of the friction element:

$$\boldsymbol{\varepsilon}^{bfp} = \boldsymbol{\varepsilon}^{fp} \tag{58}$$

The energy dissipation occurs when a bonded element breaks, and in the process, the stored elastic strain energy cannot be fully recovered, with a part of it dissipated to overcome interparticle cementation bonds and to generate new frictional slip surfaces.

The breakage's dissipated energy can be written as follows:

$$\pi^{bf} = sup\left(\boldsymbol{\sigma}^{bf} : \boldsymbol{\varepsilon}^{fp}\right) = \left(p^{f} - p^{b}\right)\varepsilon_{v}^{fp} + \left(q^{f} - q^{b}\right)\varepsilon_{s}^{fp} \tag{59}$$

Substituting the constitutive relation of the bonded element into the above gives the following:

$$\pi^{bf} = \left(p^{f} - K^{b}\varepsilon_{v}^{b}\right)\varepsilon_{v}^{fp} + \left(q^{f} - 3G^{b}\varepsilon_{s}^{b}\right)\varepsilon_{s}^{fp} \tag{60}$$

The nonlinear function for the damage process is as follows:

$$Y^{bf} = stat\left(\pi^{bf}\right) \tag{61}$$

3.4. Macroscopic Strength Criterion (Homogenization II)

From a macroscopic perspective, the constitutive model of root-reinforced soil can also be treated using the LCC method, which approximately yields the macroscopic strain energy and dissipated energy. The linearized constitutive model of the RVE for root-reinforced soil is expressed as follows:

$$\boldsymbol{\sigma} = \boldsymbol{\tau} + C^{hom} : \boldsymbol{\varepsilon} = \mathbb{C}^{hom} : \boldsymbol{\varepsilon} \tag{62}$$

where $\boldsymbol{\sigma}$, $\boldsymbol{\varepsilon}$, and $\boldsymbol{\tau}$ are the stress tensor, strain tensor, and prestress tensor of the RVE, respectively; C^{hom} is the macroscopic elastic stiffness tensor of the RVE without considering plastic deformation; $\mathbb{C}^{hom}$ is the RVE macroscopic stiffness tensor corrected by the LCC method.

From homogenization theory and based on a binary-medium model, we have the following:

$$\boldsymbol{\sigma} = \left(\mathbf{1} - \lambda^{f}\right)\boldsymbol{\sigma}^{b} + \lambda^{f}\boldsymbol{\sigma}^{f} \tag{63}$$

$$\boldsymbol{\varepsilon} = \left(\mathbf{1} - \lambda^{f}\right)\boldsymbol{\varepsilon}^{b} + \lambda^{f}\boldsymbol{\varepsilon}^{f} \tag{64}$$

Substituting the above into the constitutive relations of the RVE, the bonded element, and the friction element, we obtain the following:

$$\boldsymbol{\tau} + C^{hom} : \boldsymbol{\varepsilon} = \left(\mathbf{1} - \lambda^{f}\right)\mathbb{C}^{b} : \boldsymbol{\varepsilon}^{b} + \lambda^{f}\left(\boldsymbol{\tau}^{f} + C^{f} : \boldsymbol{\varepsilon}^{f}\right) \tag{65}$$

By substituting Equation (51) into Equation (65) and comparing, we obtain the following:

$$C^{hom} : \boldsymbol{\varepsilon} = \left(\mathbf{1} - \lambda^f\right)\mathbb{C}^b : \boldsymbol{\varepsilon}^b + \lambda^f C^f : \boldsymbol{\varepsilon}^f \tag{66}$$

$$\boldsymbol{\tau} = \lambda^f C^\tau : \boldsymbol{\varepsilon}^f \tag{67}$$

By computation via the Mori–Tanaka method, the macroscopic elastic stiffness tensor C^{hom} can be expressed as follows:

$$C^{hom} = \left(K^{hom},\, 3G^{hom}\right) \tag{68a}$$

$$K^{hom} = K^b\left[1 + \frac{\lambda^f(\frac{K^f}{K^b} - 1)}{1 + (1-\lambda^f)S_1^b(\frac{K^f}{K^b} - 1)}\right] \tag{68b}$$

$$G^{hom} = G^b\left[1 + \frac{\lambda^f\left(\frac{G^f}{G^b} - 1\right)}{1 + \left(1-\lambda^f\right)S_2^b\left(\frac{G^f}{G^b} - 1\right)}\right] \tag{68c}$$

where S_1^f and S_2^f are the coefficients of the Eshelby tensor $\mathbb{S}^f$ for the case with the friction element as the matrix and the cemented element as the inclusion, satisfying the following:

$$\mathbb{S}^b = \mathrm{S}_1^b\mathbb{J} + \mathrm{S}_2^b\mathbb{K} \tag{69a}$$

$$\mathrm{S}_1^b = \frac{3K^b}{3K^b + 4G^b} \tag{69b}$$

$$\mathrm{S}_2^b = \frac{6}{5}\frac{K^b + 2G^b}{3K^b + 4G^b} \tag{69c}$$

Similarly, the macroscopic stiffness tensor $\mathbb{C}^{hom}$ after linearization can be written as follows:

$$\mathbb{C}^{hom} = \left(\mathbb{K}^{hom},\, 3G^{hom}\right) \tag{70a}$$

$$\mathbb{K}^{hom} = K^b\left[1 + \frac{\lambda^f(\frac{\mathbb{K}^f}{K^b} - 1)}{1 + (1-\lambda^f)S_1^b(\frac{\mathbb{K}^f}{K^b} - 1)}\right] \tag{70b}$$

$$\mathbb{G}^{hom} = G^b\left[1 + \frac{\lambda^f(\frac{\mathbb{G}^f}{G^b} - 1)}{1 + (1-\lambda^f)S_2^b(\frac{\mathbb{G}^f}{G^b} - 1)}\right] \tag{70c}$$

The strain tensors of the bonded and friction elements satisfy the following:

$$\boldsymbol{\varepsilon}^b = \mathbb{A} : \boldsymbol{\varepsilon}^f \tag{71}$$

where A is the local strain concentration tensor, expressed as follows:

$$\mathbb{A} = \mathbb{I} + \mathbb{S}^b : \left(\mathbb{C}^b\right)^{-\mathbf{1}} : \left(\mathbb{C}^b - \mathbb{C}^{\mathrm{f}}\right) \tag{72}$$

The explicit expression of the local strain concentration tensor is as follows:

$$\mathbb{A} = (\mathbb{A}_1, \mathbb{A}_2) = \left(1 + \mathrm{S}_1^b\left(1 - \frac{\mathbb{K}^f}{K^b}\right), 1 + \mathrm{S}_2^b\left(1 - \frac{\mathbb{G}^f}{G^b}\right)\right) \tag{73}$$

Substituting Equation (71) into Equation (64), we can obtain the following:

$$\boldsymbol{\varepsilon} = \left[\left(1-\lambda^f\right)\mathbb{A} + \lambda^f I\right] : \boldsymbol{\varepsilon}^f = \mathbb{B} : \boldsymbol{\varepsilon}^f \tag{74}$$

The macroscopic strain energy is expressed as follows:

$$\varphi^{hom} = \frac{1}{2}\boldsymbol{\varepsilon} : C^{hom} : \boldsymbol{\varepsilon} + \boldsymbol{\tau} : \boldsymbol{\varepsilon} \tag{75}$$

For the RVE, the stress energy on the macroscopic scale is equal to the stress energy of the bonded element, the frictional element, and the dissipated energy of the breaking process in the meso-scale, and thus, according to this principle, we have the following:

$$\varphi^{hom} = \left(1-\lambda^f\right)\varphi^b + \lambda^f\varphi^f + \lambda^f\varphi^{bf} \tag{76}$$

After linearization by the LCC method, the stiffness tensors and the stress–strain tensors of the bonded element, the friction element, and the RVE are all diagonal. Substituting the relevant expressions into Equations (75) and (76) reduces them to the following:

$$\frac{1}{2}\mathbb{B} : C^{hom} : \mathbb{B} + \lambda^f C^\tau : \mathbb{B} = \frac{1}{2}\left(1-\lambda^f\right)\mathbb{A} : \mathbb{C}^{\mathrm{b}} : \mathbb{A} + \lambda^f\left(\frac{1}{2}C^f + C^\tau\right) \tag{77}$$

The above is a quadratic equation in $\mathbb{C}^f$ or C^τ. It can be solved using Equation (54), and we obtain the following:

$$D_1\left(\mathbb{C}^{\mathrm{f}}\right)^2 + D_2\mathbb{C}^{\mathrm{f}} + D_3 = 0 \tag{78a}$$

$$D_1 = \mathbb{S}^b : \left(\mathbb{C}^b\right)^{-\mathbf{1}} : \left[\frac{1}{2}\left(1-\lambda^f\right)^2 C^{hom} : \left(\mathbb{C}^b\right)^{-\mathbf{1}} : \mathbb{S}^b - \lambda^f\left(3/2-\lambda^f\right)\mathbb{I} - \frac{1}{2}\mathbb{S}^b\right] \tag{78b}$$

$$D_2 = -\left(1-\lambda^f\right)C^{hom} : \left(\mathbb{C}^b\right)^{-\mathbf{1}} : \mathbb{S}^b : \left[\mathbb{I} + \left(1-\lambda^f\right)\mathbb{S}^b\right] + \lambda^f\left(1-\lambda^f\right)\mathbb{S}^b : \left[\mathbb{I} + C^f : \left(\mathbb{C}^b\right)^{-\mathbf{1}}\right] + \mathbb{S}^b + \left(\mathbb{S}^b\right)^2 \tag{78c}$$

$$D_3 = \frac{1}{2}C^{hom} : \left[\mathbb{I} + \left(1-\lambda^f\right)\mathbb{S}^b\right]^2 - \lambda^f C^f : \left[\frac{1}{2}\mathbb{I} + \left(1-\lambda^f\right)\mathbb{S}^b\right] + \frac{1}{2}\mathbb{C}^{\mathrm{b}} : \left(\mathbb{I} + \mathbb{S}^b\right) : \left(\lambda^f\mathbb{I} - \mathbb{I} - \mathbb{S}^b\right) \tag{78d}$$

The physical meaning of $\mathbb{C}^{\mathrm{f}}$ implies that $0 \le \mathbb{C}^{\mathrm{f}} \le C^f$. Using the quadratic formula to solve for $\mathbb{C}^{\mathrm{f}}$, we select the root that satisfies its physical meaning and substitute it into subsequent calculations. Using Equations (51) and (52), the prestress tensor $\boldsymbol{\tau}^f$ and its stiffness tensor C^τ of the friction element can be calculated.

According to the LCC method and limit analysis theory, the maximum macroscopic dissipated energy of the homogenized composite is given by a stationary estimate of the macroscopic strain energy plus the volume-fraction-weighted sum of the nonlinear functions. The dissipated energy of the macroscopic RVE is as follows:

$$\pi^{hom} = stat\left[\varphi^{hom} + \left(1-\lambda^f\right)Y^b + \lambda^f Y^f + \lambda^f Y^{bf}\right] \tag{79}$$

Regarding the nonlinear functions, some previous researchers computed the stationary function at each step separately, substituted the results into Equation (79), and then performed another stationarity operation. This approach is questionable because each step's stationary value corresponds to a particular stress–strain state, and these states may not be mutually consistent. A more reasonable approach is to omit the intermediate stepwise calculations and evaluate the extremum of the stationary functional in a single step using Equation (79).

The above expression implicitly embodies the macro–meso energy equivalence principle. Substituting Equations (56), (61), and (76), which enforce equality of macro and meso strain energies, into Equation (79), the right-hand side becomes the sum of the dissipated energies at the mesoscopic scale, namely the following:

$$\pi^{hom} = stat\left(\lambda^f \pi^f + \lambda^f \pi^{bf}\right) \tag{80}$$

Substituting Equations (54), (55), and (60) into Equation (80), we can obtain the following by manipulation:

$$\pi^{hom} = \lambda^f \left[\left(p^f\right)^2 \left(\frac{1}{\mathbb{K}^f} - \frac{1}{K^f}\right)\left(2 - \frac{\mathbb{A}_1 K^b}{\mathbb{K}^f}\right) + \left(q^f\right)^2 \left(\frac{1}{3\mathbb{G}^f} - \frac{1}{3G^f}\right)\left(2 - \frac{\mathbb{A}_2 G^b}{\mathbb{G}^f}\right)\right] \tag{81}$$

The above expression must satisfy the strength criterion of the friction element; that is, find the stationary value of the expression subject to the condition in Equation (32). Substituting Equation (47) into Equation (81), solve for the point where the partial derivative is zero:

$$\frac{\partial \pi^{hom}}{\partial p^f} = 0 \tag{82}$$

Similarly, the dissipated energy at the macroscopic scale can be defined as follows:

$$\pi^{hom} = \sup(\boldsymbol{\sigma} : \boldsymbol{\varepsilon}^p) = P\varepsilon_v^p + Q\varepsilon_s^p \tag{83}$$

where P and Q are the mean stress and the principal stress difference in the RVE of root-reinforced soil at the critical failure state; $\boldsymbol{\varepsilon}^p$ is the plastic strain tensor at the critical failure state; and ε_v^p and ε_s^p are the plastic volumetric strain and plastic shear strain, which can be written as follows:

$$\boldsymbol{\varepsilon}^p = \boldsymbol{\varepsilon} - \boldsymbol{\varepsilon}^p = \left[\left(\mathbb{C}^{hom}\right)^{-1} - \left(C^{hom}\right)^{-1}\right] : \boldsymbol{\sigma} \tag{84}$$

The macroscopic dissipated energy is expressed as follows:

$$\pi^{hom} = P^2\left(\frac{1}{\mathbb{K}^{hom}} - \frac{1}{K^{hom}}\right) + Q^2\left(\frac{1}{3\mathbb{G}^{hom}} - \frac{1}{3G^{hom}}\right) \tag{85}$$

According to the macro–meso energy equivalence principle, the dissipated energies at the macroscopic and mesoscopic scales are equal, from which the macroscopic strength criterion for root-reinforced soil is ultimately obtained:

$$F^{hom} = \frac{P^2}{X_1} + \frac{Q^2}{X_2} - 1 = 0 \tag{86}$$

in which

$$X_1 = \frac{\mathbb{K}^{hom} K^{hom} R}{K^{hom} - \mathbb{K}^{hom}} \tag{87a}$$

$$X_2 = 3\frac{\mathbb{G}^{hom} G^{hom} R}{G^{hom} - \mathbb{G}^{hom}} \tag{87b}$$

$$R = \lambda^f M^2 N\left(\frac{S^2 M^2 N}{L + M^2 N} - a\right) \tag{87c}$$

$$L = \left(\frac{1}{\mathbb{K}^f} - \frac{1}{K^f}\right)\left(2 - \frac{\mathbb{A}_1 K^b}{\mathbb{K}^f}\right) \tag{87d}$$

$$N = \left(\frac{1}{3\mathbb{G}^f} - \frac{1}{3G^f}\right)\left(2 - \frac{\mathbb{A}_2 G^b}{\mathbb{G}^f}\right) \tag{87e}$$

4. Verification of Strength Criterion

4.1. Determination of Strength Parameters

To predict the strength of root-reinforced soil under freeze–thaw cycling, it is necessary to know the parameters of the roots, the cemented-soil matrix, and the friction elements, as well as the breakage parameter. The bulk modulus K^r and shear modulus G^r of the roots can be determined directly through laboratory compression tests. In the binary-medium model, it can be considered that at the initial stage of loading, the specimen is mainly composed of bonded elements, and the breakage ratio is low. Therefore, the bulk modulus K^{bm} and shear modulus G^{bm} of the cemented-soil matrix can be approximately determined from the initial slopes of the $\varepsilon_v - \sigma_m$ and $\varepsilon_s - \sigma_s$ curves at 0.2% axial strain in conventional triaxial tests on specimens without roots and subjected to no freeze–thawing cycling.

After completion of the triaxial test, the bonded elements are essentially completely damaged; the remolded soil after freeze–thaw and triaxial testing consists predominantly of friction elements. The parameters of the friction elements can be obtained from triaxial tests on the remolded specimens after freeze–thaw and triaxial testing. The elastic bulk and shear moduli K^f and G^f of the friction elements can be approximately determined from the initial slopes of the $\varepsilon_v^f - \sigma_m^f$ and $\varepsilon_s^f - \sigma_s^f$ curves of these remolded specimens. The parameters a, S, and M, reflecting the strength of the friction elements, can be obtained by comparing the tested and computed results of the strengths measured on the remolded specimens experienced by trial and error or optimizing methods of the freeze–thawing process.

For the breakage ratio denoting the degree of breakage of the bonded element upon loading and ranging from 0 to 1.0 of its value, many studies have shown that its evolution follows a Weibull distribution function [39]. We recommend the following equation:

$$\lambda^f = 1 - exp\left[-\alpha\left(\frac{P}{P_a}\right)^{\beta}\right] \tag{88}$$

where α and β are breakage-fraction parameters that can be determined by trial and error, and Pa is the standard atmospheric pressure.

4.2. Experimental Verification

The test soil was extracted from Hailuogou, in the Sichuan Province of China, at an elevation of about 3000 m, from a depth of 0.5–1.0 m below the ground surface [26]. The soil is a silty sand, and the roots used were from rowan (*Sorbus*). The roots were about 5 cm long with a diameter of about 5 mm; the mass of a single root was about 1.4 g, corresponding to a mass fraction of 0.292% (on a dry-mass basis), a volume fraction of 0.262%, and a shearing-area fraction of 0.254%. Specimens were prepared at a target dry density of 1.28 g/cm^3, with a diameter of 61.8 mm and a height of 125 mm. After specimen preparation, they were vacuumed for 2 h and then submerged to saturate in water for more than 12 h. Specimens not subjected to freeze–thaw cycles were tested directly in triaxial compression; for specimens requiring freeze–thaw cycles, they were promptly placed in water to remove bubbles and transferred under water into lidless transparent plastic jars. The jars containing the specimens were labeled and placed in a fully automatic low-temperature freeze–thaw machine to begin cycling. During the freeze–thaw cycles, water could be replenished through the porous stones at the top and bottom ends of the specimen. According to the temperature of the field, one freeze–thaw cycle consisted of cooling from room temperature to −15 °C and holding for 12 h, then heating to 20 °C and holding for 12 h. After the

prescribed number of cycles, the specimen was mounted on a triaxial apparatus and tested under room-temperature consolidated drained conditions, with an axial loading rate of 0.1 mm/min and confining pressures of 25, 50, 100, and 200 kPa. The test was terminated when the axial strain reached 15%, which was taken as failure. The test matrix included confining pressures of 25 kPa, 50 kPa, 100 kPa, and 200 kPa; freeze–thaw cycle counts of 0, 1, 5, and 15; and root counts of none, one root, and three roots.

Based on the triaxial test results, the bulk and shear moduli of the roots, the cemented-soil matrix, and the frictional element were determined. From the strengths of remolded specimens after freeze–thaw and triaxial testing, the strength parameters a, S, and M of the frictional element were fitted. A computational program was then developed to verify the strength criterion for root-reinforced soils, which are as follows: Step 1: Inputting the model parameters K^{bm}, G^{bm}, K^r, G^r, K^f,G^f, a, S, M, α, β, and P_a; Step 2: Solving K^b, G^b, and $\mathbb{S}^{bm}$, C^{bm}, $\mathbb{A}$, $\mathbb{B}$ using the parameters of the bonded element that were obtained using the Mori–Tanaka method; Step 3: Solving D_1, D_2, and D_3 according to strain-energy conservation, and then solving $\mathbb{C}^b - \mathbb{C}^f$, $\mathbb{C}^f$, $\mathbb{C}^r$; Step 4: Determining the reasonable range of $\mathbb{C}^f$, and discarding meaningless roots; Step 5: Obtaining the relevant parameters $\mathbb{C}^{hom}$, X_1, X_2 for the macroscopic strength criterion; Step 6: Solving the corresponding P and Q. Under triaxial stress, the mean stress P and the principal stress difference Q are as follows:

$$P = \sigma_3 + \frac{1}{3}(\sigma_1 - \sigma_3) \tag{89}$$

$$Q = \sigma_1 - \sigma_3 \tag{90}$$

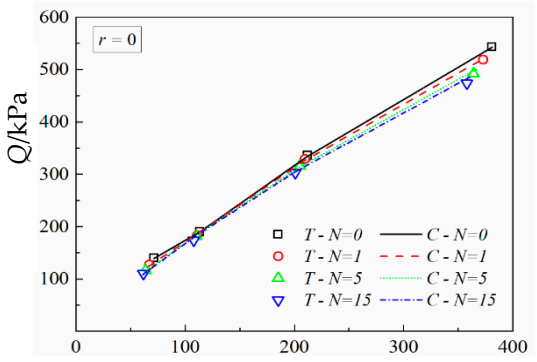
Following the parameter determination procedure described above, the parameters of the strength criterion for root-reinforced soil under freeze–thaw action were ultimately identified by fitting the test data and performing inverse analysis; these are listed in Table 1. Among them, the damage-rate parameter is affected by the number of freezing–thaw cycles: as the number of cycles increases, the parameter α increases and the damage rate rises accordingly, which corroborates the conclusion that freeze–thaw cycling exacerbates damage to the bonded element.

Table 1. Parameters of strength criterion.

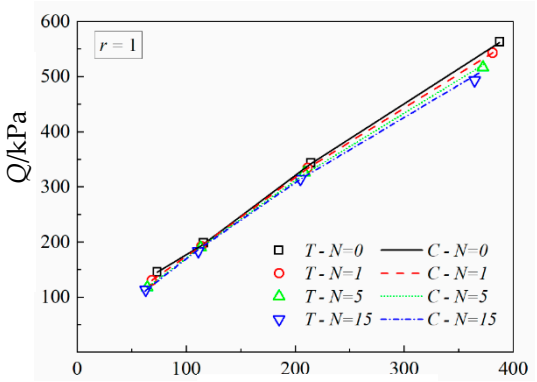
Parameters	Symbol	Value	Determining Method
Bonded element	K^{bm}/kPa	$P_a\left[83720\left(\frac{\sigma_3}{P_a}\right)^{0.00111} - 83513\right]$	Triaxial tests of the samples without roots and without freeze–thaw cycling at 0.2% axial strain
	G^{bm}/kPa	$P_a\left[12470\left(\frac{\sigma_3}{P_a}\right)^{0.00282} - 12376\right]$	
	K^r/kPa	135,000	Directly through laboratory compression tests
	G^r/kPa	20,250	
Frictional elements	K^f/kPa	$P_a\left[17530\left(\frac{\sigma_3}{P_a}\right)^{0.00156} - 17439\right]$	Triaxial tests of the remolded samples
	G^f/kPa	$P_a\left[109.1\left(\frac{\sigma_3}{P_a}\right)^{0.3696} - 46.08\right]$	
	a	0.01	By comparing the tested and computed results, fitting of the strengths measured on the remolded specimens is achieved by trial and error or optimization methods
	M	1.185	
	S/kPa	42.72	
Breakage ratio	α	$0.00108\ln(4.5\mathrm{N} + 2.623) + 0.2909$	By trial and error
	β	0.155	

Based on the parameters in Table 1, the strength criterion model for root-reinforced soil was used to predict strengths under different confining pressures, numbers of freeze–thaw cycles, and root contents, as shown in Figures 3 and 4, in which each data point represents the average of the peak stress–strain curves (or specific strain) obtained from three parallel triaxial tests conducted under the same confining pressure and density

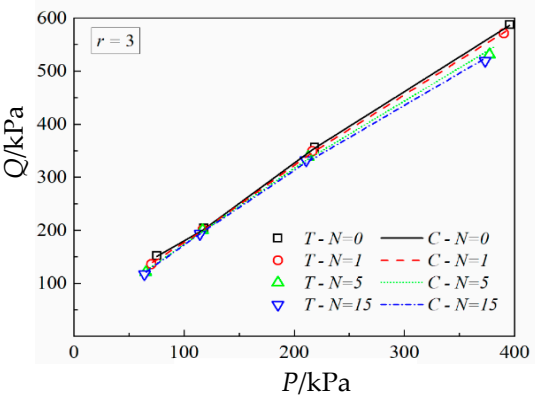
conditions. Figures 3 and 4 indicate that the model-predicted trends of strength for root-reinforced soil under freeze–thaw action are consistent with the experimental results: strength increases with increasing confining pressure, decreases with increasing numbers of freeze–thaw cycles, and increases with higher root content. A comparison between the model predictions and the test data shows that the model can reproduce, with good accuracy, both the magnitude of strength and its variation under freeze–thaw cycling, with small prediction errors.



(**a**) r = 0 (no root)

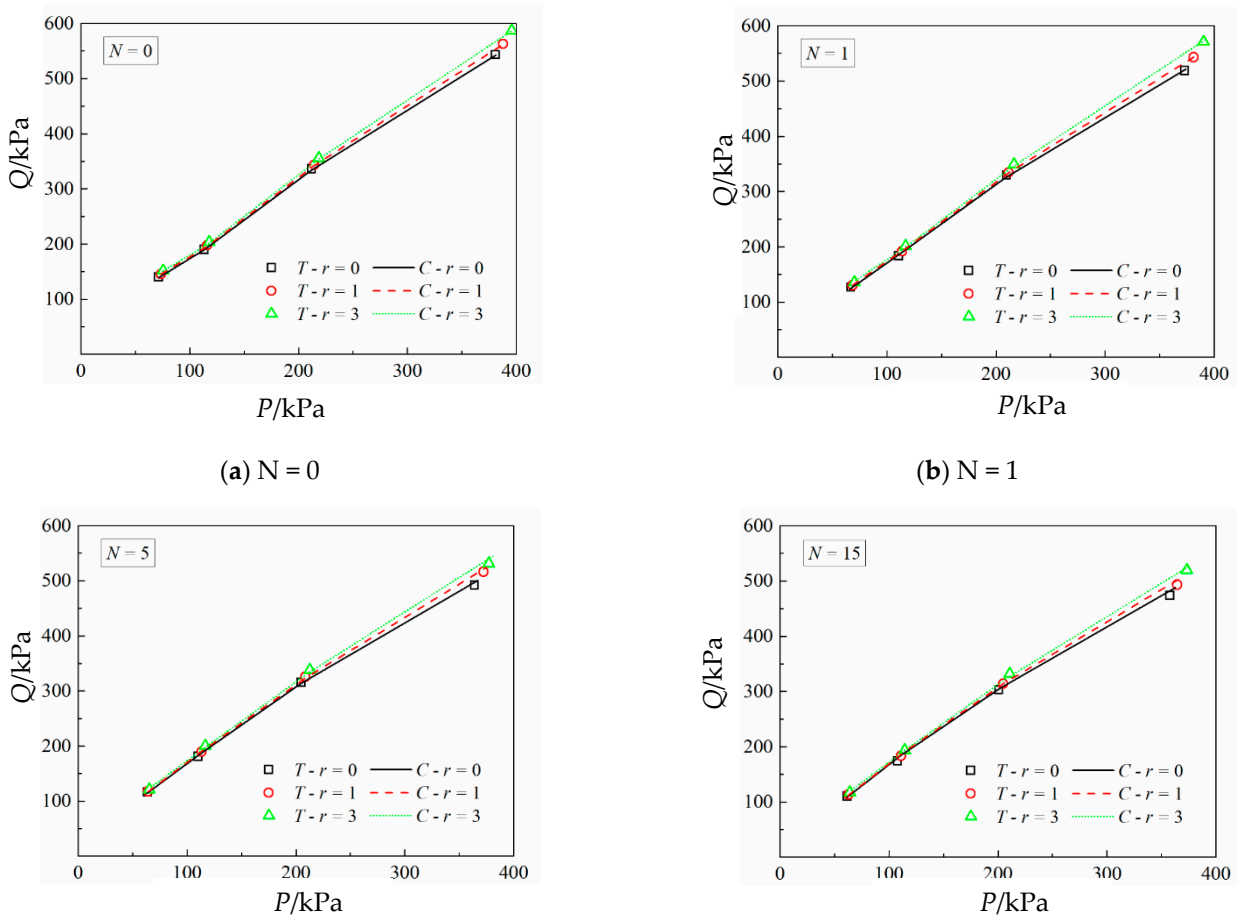


(**b**) r = 1 (one root)



(**c**) r = 3 (3 roots)

Figure 3. Comparison of strength predictions and test results under different numbers of freeze–thaw cycles (T: Tested; C: Computed; N: the number of freezing–thawing cycles).



(**a**) N = 0 (**b**) N = 1

(**c**) N = 5 (**d**) N = 15

Figure 4. Comparison of strength predictions and test results for different root contents (T: Tested; C: Computed; r: the number of roots; N: the number of freezing–thawing cycles).

The proposed strength criterion model is derived on a micromechanical scale and can reasonably capture the micromechanical failure mechanisms of a three-constituent composite. The model requires relatively few parameters, and their physical meanings are clear; except for the damage-rate parameter, the parameters for the cemented-soil matrix, the frictional element, and the roots can all be obtained from laboratory tests. In summary, the micromechanics-based strength criterion for root-reinforced soils, which accounts for the effects of freeze–thaw cycling, can provide a reliable basis for engineering practice.

5. Conclusions

A new strength criterion for root-reinforced soil has been developed, accounting for the number of freeze–thaw cycles. This criterion was derived in two steps using a homogenization approach and was then used to predict soil strengths, which were compared against experimental results. The main findings are summarized as follows:

(i) The strength criterion model for root-reinforced soil treats the bonded element as the matrix and the frictional element as the inclusion. The bonded element consists of a cemented-soil matrix with root inclusions. This model, based on a micromechanical perspective, represents a three-constituent composite. By combining the binary-medium model, micromechanics, macro–micro energy equivalence, and limit analysis, a macroscopic strength criterion for the root-reinforced soil representative volume element (RVE) was derived, revealing the breakage mechanisms at the microscale. This approach overcomes the limitations of previous limit analysis applications. Through the Mori–Tanaka method

and macro–micro strain-energy equivalence, it inversely determines the prestress and moduli of the linearized frictional element.

(ii) Most parameters in the strength criterion have clear physical meanings and can be determined through microscale tests, except for the parameters related to the breakage ratio, which follow a Weibull distribution. These parameters are determined by comparing them with experimental results. Using the proposed strength criterion model, strengths under different confining pressures, numbers of freeze–thaw cycles, and root contents were predicted with good accuracy, consistent with the trends observed in root-reinforced soil tests.

Although the new strength criterion offers advantages over existing macro-based strength criteria, its derivation process is relatively complex, and the parameter determination method needs further refinement for root-reinforced soil; for instance, the strength parameters of the frictional elements and the parameters of the breakage ratio can be determined by optimizing methods or machine learning methods. In addition, the freezing–thawing actions also affect the model parameters of the bonded and frictional elements; and in this paper, roots are assumed to be elastic, which is greatly distinct from real roots that are inelastic, have large deformation, and are anisotropic, and these topics can be further studied in the future.

Author Contributions: W.L.: writing—original draft, investigation, validation, visualization, and formal analysis. F.C.: writing—review and editing, investigation, data curation, conceptualization, and supervision. Y.W.: resources. G.X.: data curation. E.L.: conceptualization, methodology, writing—review and editing, and supervision. All authors have read and agreed to the published version of the manuscript.

Funding: This research received financial support from Science and Technology Projects of Xizang Autonomous Region, China (Grant No. XZ202501ZR0092).

Data Availability Statement: The original contributions presented in this study are included in the article. Further inquiries should be directed to the corresponding authors.

Conflicts of Interest: Authors Wei Luo, Yang Wang and Guiyou Xiao were employed by the company Tibet Development Investment Group Co., Ltd. Author Fu Cao was employed by the company PowerChina HydroPower Development Group Co., Ltd. The remaining author declares that the research was conducted in the absence of any commercial or financial relationships that could be construed as a potential conflict of interest.

Appendix A. Deriving the Strain Concentration Tensors of Equation (17)

The bonded element consists of the cemented-soil matrix and root inclusion, and both of them behave elastically.

Eshelby first studied the phase change strain problem ε^t in an infinite homogeneous medium $\boldsymbol{\Omega}$, where the material within region H experiences phase changes, temperature variations, cracks, dislocations, inhomogeneities, and other causes [27]. Mura referred to $\boldsymbol{\varepsilon}^t$ as the characteristic strain, which is a constant tensor [29]. When the material in region H is free and unconstrained, its strain is the characteristic strain $\boldsymbol{\varepsilon}^t$. Outside of region H, in the infinite homogeneous medium $\boldsymbol{\Omega}$, the characteristic strain or corresponding initial stress is zero, and the displacement tends to zero at infinity. The material in region H with characteristic strain $\boldsymbol{\varepsilon}^t$ is equivalent to the applied initial stress $\boldsymbol{p}^H = -\mathbb{C} : \boldsymbol{\varepsilon}^t$, and the static possible stress field $\boldsymbol{\sigma}^*$ satisfies Equation (A1), where $\boldsymbol{\varepsilon}^*$ is the possible strain field and $\mathbb{C}$ is the stiffness tensor of the infinite medium:

$$\boldsymbol{\sigma}^* = \mathbb{C} : \left(\boldsymbol{\varepsilon}^* - \boldsymbol{\varepsilon}^t\right) \; x \in H \tag{A1a}$$

$$\boldsymbol{\sigma}^* = \mathbb{C} : \boldsymbol{\varepsilon}^* \; x \in (\boldsymbol{\Omega} - H) \tag{A1b}$$

In reality, region H cannot deform freely; it is constrained by the surrounding infinite homogeneous medium. Due to the presence of this constraint, the deformation of region H is limited, and the actual strain is referred to as the constrained strain.

Mura and Cheng [28] proved that, when the infinite homogeneous medium is linearly elastic, and the shape of region H is an ellipsoid, the characteristic strain $\boldsymbol{\varepsilon}^*$, as long as it is a constant tensor (i.e., it does not vary with position in region H), will result in the constrained strain $\boldsymbol{\varepsilon}^*$ in region H, which is also a constant tensor. Its value is as follows:

$$\boldsymbol{\varepsilon}^* = \mathbb{S} : \boldsymbol{\varepsilon}^t \left(= -\mathbb{P} : \boldsymbol{p}^H \right) \tag{A2a}$$

$$\mathbb{S} = \mathbb{P} : \mathbb{C} \tag{A2b}$$

where $\mathbb{S}$ is called the Eshelby tensor, which is a fourth-order tensor. The Eshelby tensor can be determined through elastic mechanics by using the Green's function of the isotropic linear elastic infinite medium. It is related to the shape, orientation, and stiffness of the infinite medium surrounding the ellipsoidal region H. When region H is spherical, the expression for the Eshelby tensor is derived as follows:

$$\mathbb{S} = \mathrm{S}_1 \mathbb{J} + \mathrm{S}_2 \mathbb{K} \tag{A3a}$$

$$\mathbb{I}_{ijkl} = \frac{1}{2}\left(\delta_{ik}\delta_{jl} + \delta_{il}\delta_{jk} \right) \tag{A3b}$$

$$\mathbb{J}_{ijkl} = \frac{1}{3}\delta_{ij}\delta_{kl} \tag{A3c}$$

$$\mathbb{K} = \mathbb{I} - \mathbb{J} \tag{A3d}$$

$$\mathrm{S}_1 = \frac{3K}{3K + 4G} = \frac{1+\nu}{3(1-\nu)} \tag{A3e}$$

$$\mathrm{S}_2 = \frac{6}{5}\frac{K + 2G}{3K + 4G} = \frac{2}{15}\frac{4 - 5\nu}{1 - \nu} \tag{A3f}$$

$$\nu = \frac{3K - 2G}{6K + 2G} \tag{A3g}$$

where $\mathbb{I}$ is the fourth-order identity tensor, $\mathbb{J}$ is the fourth-order spherical tensor, and K and G are the bulk and shear moduli, respectively, of the infinite homogeneous medium, and ν is the Poisson's ratio. $\mathbb{P}$ is the polarization tensor, which corresponds to the Eshelby tensor and satisfies Equation (A2).

In an infinite homogeneous linear elastic medium containing an inclusion, the boundary condition is a uniform strain $\underline{\varepsilon}$ at infinity. The region H, also called the inner domain, where the inclusion is located, has a stiffness of $\mathbb{C}^H$. The region outside H, called the outer domain $\boldsymbol{\Omega}$, has a stiffness of $\mathbb{C}$. The inner and outer domains are made of different materials, and displacement continuity at the interface ∂H means complete contact, as shown in Figure A1. The control equations are as follows:

$$\mathrm{div}\left(\mathbb{C} : \boldsymbol{\varepsilon}^H \right) + \mathrm{div}\left(\left(\mathbb{C}^H - \mathbb{C} \right) : \boldsymbol{\varepsilon}^H \right) = 0 \; x \in H \tag{A4}$$

$$\mathrm{div}\left(\mathbb{C} : \boldsymbol{\varepsilon}^H \right) = 0 \; x \in (\boldsymbol{\Omega} - H) \tag{A5}$$

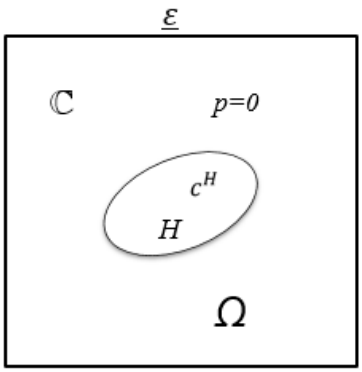


Figure A1. Inclusion problem [30].

The solution to Equations (A4) and (A5) can be expressed as a superposition of the solution for uniform strain and characteristic strain:

$$\boldsymbol{\varepsilon}^H = \underline{\boldsymbol{\varepsilon}} + \boldsymbol{\varepsilon}^* = \underline{\boldsymbol{\varepsilon}} + \mathbb{S} : \boldsymbol{\varepsilon}^t = \underline{\boldsymbol{\varepsilon}} - \mathbb{P} : \boldsymbol{p}^H \tag{A6}$$

For the inclusion problem, Equation (A5) satisfies the following:

$$\boldsymbol{p}^H = \left(\mathbb{C}^H - \mathbb{C}\right) : \boldsymbol{\varepsilon}^H \tag{A7}$$

Substituting Equation (A6) into Equation (A7) gives the following:

$$\boldsymbol{\varepsilon}^H = \left[\mathbb{I} + \mathbb{P} : \left(\boldsymbol{c}^H - \mathbb{C}\right)\right]^{-1} : \underline{\boldsymbol{\varepsilon}} \tag{A8}$$

$$\boldsymbol{\sigma}^H = \boldsymbol{c}^H : \left[\mathbb{I} + \mathbb{P} : \left(\boldsymbol{c}^H - \mathbb{C}\right)\right]^{-1} : \underline{\boldsymbol{\varepsilon}} \tag{A9}$$

From Equation (A2), we know the following:

$$\mathbb{P} = \mathbb{S} : \mathbb{C}^{-1} \tag{A10}$$

For the inclusion problem, the inner domain is constrained by the external medium and cannot deform freely according to the characteristic strain $\boldsymbol{\varepsilon}^t$; it can only deform according to $\boldsymbol{\varepsilon}^*$. Following Eshelby's method, the strain due to the internal stress $\boldsymbol{\sigma}^*$ is the constrained strain minus the characteristic strain. Using Equations (A1) and (A2), the elastic constitutive relation for the inner domain is as follows:

$$\boldsymbol{\sigma}^* = \mathbb{C} : \left(\boldsymbol{\varepsilon}^* - \boldsymbol{\varepsilon}^t\right) = -\mathbb{C} : \left(\mathbb{S}^{-1} - \mathbb{I}\right) : \boldsymbol{\varepsilon}^* = -\mathbb{C}^* : \boldsymbol{\varepsilon}^* \tag{A11}$$

where $\mathbb{C}^*$ is called the elastic constraint tensor, given by the following:

$$\mathbb{C}^* = \mathbb{C} : \left(\mathbb{S}^{-1} - \mathbb{I}\right) \tag{A12}$$

References

1. Wan, Y.; Xue, Q.; Liu, L.; Zhao, L.Y. The role of roots in the stability of landfill clay covers under the effect of dry–wet cycles. *Environ. Earth Sci.* **2016**, *75*, 71. [CrossRef]
2. Lian, B.; Peng, J.; Zhan, H.; Wang, X. Mechanical response of root-reinforced loess with various water contents. *Soil Tillage Res.* **2019**, *193*, 85–94. [CrossRef]
3. Feng, B.; Zong, Q.; Cai, H.; Chen, Z.; Wang, J. Calculation of increased soil shear strength from desert plant roots. *Arab. J. Geosci.* **2019**, *12*, 525. [CrossRef]
4. Wang, Y.; Liu, X.; Zhang, Z.; Ma, D.; Cui, Y. Experimental study on the influence of root content on the strength of undisturbed and remolded grass-root-reinforced soils. *Chin. J. Geotech. Eng.* **2015**, *37*, 1405–1410. (In Chinese) [CrossRef]

5. Hamidifar, H.; Keshavarzi, A.; Truong, P. Enhancement of river bank shear strength parameters using Vetiver grass root system. *Arab. J. Geosci.* **2018**, *11*, 611. [CrossRef]
6. Maffra, C.; Sousa, R.; Sutili, F.; Pinheiro, R. The effect of roots on the shear strength of texturally distinct soils. *Floresta Ambiente* **2019**, *26*, e20171018. [CrossRef]
7. Cardoza, R.; Oka, L. Measuring the Effect of Grass Roots on Shear Strength Parameters of Sandy Soils. In *Geo-Congress 2020*; American Society of Civil Engineers: Reston, VA, USA, 2020.
8. Zhang, L.; Sun, J.; Shi, C. Numerical simulation on the influence of plant root morphology on shear strength in the sandy soil, Northwest China. *J. Arid Land* **2024**, *16*, 1444–1462. [CrossRef]
9. Fan, C.C.; Su, C.F. Role of roots in the shear strength of root-reinforced soils with high moisture content. *Ecol. Eng.* **2008**, *33*, 157–166. [CrossRef]
10. Liu, Y.; Hu, X.; Yu, D.; Zhu, H.; Li, G. Influence of the roots of mixed-planting species on the shear strength of saline loess soil. *J. Mt. Sci.* **2021**, *18*, 806–818. [CrossRef]
11. Gonzalez-Ollauri, A.; Mickovski, S.B. Plant-soil reinforcement response under different soil hydrological regimes. *Geoderma* **2017**, *285*, 141–150. [CrossRef]
12. Kamei, T.; Ahmed, A.; Shibi, T. Effect of freeze–thaw cycles on durability and strength of very soft clay soil stabilised with recycled Bassanite. *Cold Reg. Sci. Technol.* **2012**, *82*, 124–129. [CrossRef]
13. Aldaood, A.; Bouasker, M.; Al-Mukhtar, M. Impact of freeze–thaw cycles on mechanical behaviour of lime stabilized gypseous soils. *Cold Reg. Sci. Technol.* **2014**, *99*, 38–45. [CrossRef]
14. Han, Y.; Wang, Q.; Wang, N.; Wang, J.; Zhang, X.; Cheng, S.; Kong, Y. Effect of freeze-thaw cycles on shear strength of saline soil. *Cold Reg. Sci. Technol.* **2018**, *154*, 42–53. [CrossRef]
15. Ma, Q.; Ma, D.; Yao, Z. Influence of freeze-thaw cycles on dynamic compressive strength and energy distribution of soft rock specimen. *Cold Reg. Sci. Technol.* **2018**, *153*, 10–17. [CrossRef]
16. Xu, J.; Li, Y.; Lan, W.; Wang, S. Shear strength and damage mechanism of saline intact loess after freeze-thaw cycling. *Cold Reg. Sci. Technol.* **2019**, *164*, 102779. [CrossRef]
17. Qu, Y.; Chen, G.; Niu, F.; Ni, W.; Mu, Y.; Luo, J. Effect of freeze-thaw cycles on uniaxial mechanical properties of cohesive coarse-grained soils. *J. Mt. Sci.* **2019**, *16*, 2159–2170. [CrossRef]
18. Fish, A.M. Thermodynamic model of creep at constant stress and constant strain rate. *Cold Reg. Sci. Technol.* **1984**, *9*, 143–161. [CrossRef]
19. Chen, D.; Wang, D.; Ma, W.; Lei, L.; Li, G. A strength criterion for frozen clay considering the influence of stress Lode angle. *Can. Geotech. J.* **2019**, *56*, 1557–1572. [CrossRef]
20. Liao, M.; Lai, Y.; Wang, C. A strength criterion for frozen sodium sulfate saline soil. *Can. Geotech. J.* **2016**, *53*, 1176–1185. [CrossRef]
21. Liu, X.; Liu, E. Application of new twin-shear unified strength criterion to frozen soil. *Cold Reg. Sci. Technol.* **2019**, *167*, 102857. [CrossRef]
22. Luo, F.; Liu, E.; Zhu, Z. A strength criterion for frozen moraine soils. *Cold Reg. Sci. Technol.* **2019**, *164*, 102786. [CrossRef]
23. Zhou, M.M.; Meschke, G. A multiscale homogenization model for strength predictions of fully and partially frozen soils. *Acta Geotech.* **2018**, *13*, 175–193. [CrossRef]
24. Mori, T.; Tanaka, K. Average stress in matrix and average elastic energy of materials with misfitting inclusions. *Acta Metall.* **1973**, *21*, 571–574. [CrossRef]
25. Ortega, J.A.; Gathier, B.; Ulm, F.J. Homogenization of cohesive-frictional strength properties of porous composites: Linear comparison composite approach. *J. Nanomech. Micromech.* **2011**, *1*, 11–23. [CrossRef]
26. Luo, W.; Xiang, B.; Liu, E.; Zhao, H.; Wu, K.; He, Y. Mechanical properties of rooted soil under freeze–thaw cycles and extended binary medium constitutive model. *Sci. Rep.* **2023**, *13*, 13607. [CrossRef]
27. Eshelby, J.D. The Determination of the elastic field of an ellipsoidal inclusion, and related problems. *Proc. R. Soc. A Math. Phys. Eng. Sci.* **1957**, *241*, 376–396. [CrossRef]
28. Mura, T.; Cheng, P.C. The Elastic Field Outside an Ellipsoidal Inclusion. *J. Appl. Mech.* **1959**, *252*, 561–569. [CrossRef]
29. Mura, T. *Micromechanics of Defects in Solids*; Springer Science & Business Media: Berlin/Heidelberg, Germany, 1987.
30. Zhang, Y.; Zhang, Z. *Mesomechanics of Materials*; Science Press: Beijing, China, 2008.
31. Zhao, L.Y.; Zhu, Q.Z.; Shao, J.F. A micro-mechanics based plastic damage model for quasi-brittle materials under a large range of compressive stress. *Int. J. Plast.* **2018**, *100*, 156–176. [CrossRef]
32. Castaneda, P.P. Second-order homogenization estimates for nonlinear composites incorporating field fluctuations: I—Theory. *J. Mech. Phys. Solids* **2002**, *50*, 737–757. [CrossRef]
33. Lopez-Pamies, O.; Ponte Castaneda, P. Second-order homogenization estimates incorporating field fluctuations in finite elasticity. *Math. Mech. Solids* **2004**, *9*, 243–270. [CrossRef]
34. Wang, P.; Liu, E.; Zhi, B. An elastic-plastic model for frozen soil from micro to macro scale. *Appl. Math. Model.* **2021**, *91*, 125–148. [CrossRef]

35. Dormieux, L.; Molinari, A.; Kondo, D. Micromechanical approach to the behavior of poroelastic materials. *J. Mech. Phys. Solids* **2002**, *50*, 2203–2231. [CrossRef]
36. Dormieux, L.; Lemarchand, E.; Kondo, D.; Brach, S. Strength criterion of porous media: Application of homogenization techniques. *J. Rock Mech. Geotech. Eng.* **2017**, *9*, 62–73. [CrossRef]
37. Dormieux, L.; Kondo, D.; Ulm, F.-J. *Microporomechanics*; John Wiley & Sons, Ltd.: Hoboken, NJ, USA, 2006.
38. Maghous, S.; Dormieux, L.; Barthelemy, J.F. Micromechanical approach to the strength properties of frictional geomaterials. *Eur. J. Mech.-A/Solids* **2009**, *28*, 179–188. [CrossRef]
39. Liu, E.; Yu, H.-S.; Zhou, C.; Nie, Q.; Luo, K. A binary-medium constitutive model for artificially structured soils based on the disturbed state concept (DSC) and homogenization theory. *Int. J. Geomech.* **2017**, *17*, 04016154. [CrossRef]

Disclaimer/Publisher's Note: The statements, opinions and data contained in all publications are solely those of the individual author(s) and contributor(s) and not of MDPI and/or the editor(s). MDPI and/or the editor(s) disclaim responsibility for any injury to people or property resulting from any ideas, methods, instructions or products referred to in the content.